Bioorganic & Medicinal Chemistry 17 (2009) 4921–4927

Contents lists available at ScienceDirect

Bioorganic & Medicinal Chemistry

journal homepage: www.elsevier.com/locate/bmc

Nucleoside–amino acid conjugates: An alternative route to the design of ribonuclease A inhibitors

Joy Debnath, Swagata Dasgupta *, Tanmaya Pathak *

Department of Chemistry, Indian Institute of Technology, Kharagpur, Kharagpur 721 302, India

ARTICLE INFO

Article history:
Received 18 April 2009
Revised 1 June 2009
Accepted 2 June 2009
Available online 6 June 2009

Keywords:
Nucleoside–amino acid conjugate
Ribonuclease A inhibitor
Agarose gel
Kinetics
Docking

ABSTRACT

Nucleoside–amino acid conjugates have been employed to inhibit the ribonucleolytic activity of ribonuclease A (RNase A) and affect the protonation/deprotonation equilibrium of its active site histidine residues. Agarose gel and precipitation assays indicate inhibition of RNase A activity by these molecules with a possible role of the polar side chains of the amino acids in RNase A inhibition. Kinetic experiments demonstrated that the mode of inhibition is competitive in nature with inhibition constants (K_i) in the micromolar range. The nucleoside–serine conjugate occupies the active site of RNase A and preferential perturbs the pK_a value of His-119 by its 'free amino group' as found from ^{1}H NMR studies. Docking studies revealed that the free amino groups of the most active compounds are within hydrogen bonding distance of His-119 in inhibitor–RNase A complexes.

1. Introduction

Ribonucleases become cytotoxic when they adsorb specifically to certain cells, enter the cytosol, degrade RNA and consequently inhibit protein syntheses leading to cell death. Progress in ribonuclease inhibition studies has increased over the years to limit the nefarious biological activities of some of the ribonuclease superfamily proteins such as angiogenin,[1] eosinophil-derived neurotoxin (EDN),[2] and bovine seminal RNase.[3] All these proteins bear active site homology with ribonuclease A (RNase A),[4–6] a model protein of this superfamily. The biological activities of these proteins are also very much dependent on their ribonucleolytic activity.[7] Thus inhibitors which can inhibit RNase A by targeting its ribonucleolytic site, can also lead to inhibition of other ribonuclease homologues. Therefore ribonuclease inhibitors have been intensively sought after for therapeutic purposes. The ribonucleolytic center of RNase A is comprised of multiple subsites which bind the phosphate, base, and sugar components of RNA.[8,9] Among them, the P_1 subsite is designated for cleavage of the phosphodiester bond. His-12, Lys-41 and His-119 serve as the catalytic residues at the P_1 subsite (Fig. 1). The B_1 and B_2 sites recognize the nucleobases whose ribose sugar unit is attached to the phosphate group via the 3′- and 5′-oxygen atom, respectively. Generally the B_1 site shows pyrimidine specificity whereas the B_2 site has purine affinity.[10]

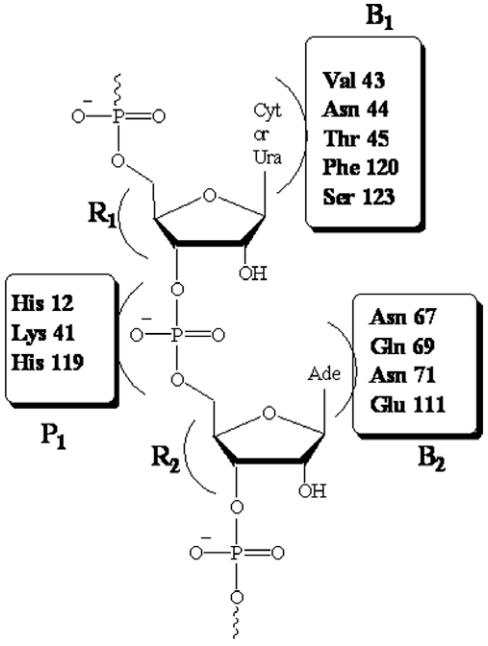

Figure 1. Key residues of the active site of RNase A.

Several nucleoside-based inhibitors of RNase A functionalized with phosphate or pyrophosphate, which are substrate mimics inhibit the ribonucleolytic activity of the enzyme effectively.[9,11]

* Corresponding authors. Tel.: +91 3222 283306; fax: +91 3222 255303 (S.D.); tel.: +91 3222 283342; fax: +91 3222 255303 (T.P.).
E-mail addresses: swagata@chem.iitkgp.ernet.in (S. Dasgupta), tpathak@chem.iitkgp.ernet.in (T. Pathak).

0968-0896/$ - see front matter © 2009 Elsevier Ltd. All rights reserved.
doi:10.1016/j.bmc.2009.06.002

However, the major problem associated with these compounds is their transport across biological membranes. The high negative charge on the phosphate group makes them difficult to use in vivo.[12] In case of reported RNase A inhibitors, which are functionalized with acidic groups (phosphate, carboxylic or sulfonic), it is expected that they would exist in the deprotonated form at physiological pH and would therefore disrupt the normal acid-base equilibrium at the P_1 site. Aminonucleosides as inhibitors of RNase A have been studied[13,14] since it is known that the pK_a of His-12 and His-119 of RNase A changes from ~5.22/6.78 for free enzyme to ~6.30/8.10 for enzyme–substrate complexes.[15] Thus the introduction of a primary amino group with a comparatively higher pK_a value should also disrupt the normal acid-base equilibrium of active site.

In this report we have argued that nucleosides functionalized with a 'free amino group', with p$K_a \sim 9$–10 should perturb the microenvironment of the histidine residues of RNase A present at the P_1 site. This in turn would diminish the ribonucleolytic activity of RNase A in a different mode as exhibited by the presence of a phosphate moiety. As His-12 and His-119 contribute significantly to the stability of the RNase A-single stranded nucleic acid complex, it is likely that stronger amino groups delivered to the P_1 site by an appropriately functionalized pyrimidine nucleoside, would bind with RNase A and perturb the histidine residues responsible for its catalytic activity.[9] It is known that the 2′-OH group contributes significantly towards the conformational preferences of the furanose ring. Nevertheless, we selected thymidine derivatives as model compounds for this study because of the easier synthetic manipulations required for accessing the final conjugates due to the absence of the 2′-OH group.

2. Results and discussion

We report here for the first time the use of nucleoside–amino acid conjugates as effective inhibitors (Scheme 1) of the ribonucleolytic activity of RNase A. Since our intention was to deliver a 'free amino group' through a spacer to the P_1 site of the enzyme, we have selected an amide linkage because of its easy synthesis and known stability towards the ribonucleolytic activity of RNase A. We also opined that the structurally varied nucleoside–amino acid conjugates, which can be synthesized by coupling the amino group of aminonucleosides and the carboxylic function of an amino acid, would deliver the amino group embedded in a range of hydrophilic and hydrophobic environments to the P_1 site of RNase A. It is expected that the series of nucleoside–amino acid conjugates with different side chains in the amino acid part of the molecule would also help us in identifying the contributions of other factors such as steric bulk, hydrophobicity and chirality around the amino group, in proper positioning of the amino function near the histidine residues at the P_1 site.

The inhibition of the ribonucleolytic activity of RNase A was initially checked qualitatively by an agarose gel based assay, where the degradation of tRNA by RNase A was monitored. The most intense band observed in lane 1 is due to the presence of the control, tRNA. The maximum possible degradation of tRNA by RNase A results in the faint intensity of the band observed in lane 2 (Fig. 2). The differential intensity of bands in lanes 3–5 indicates the extent of RNase A inhibition by the compounds at three different concentrations (higher to lower concentrations, respectively). These results qualitatively show better inhibition potency of **Ser-aT**, **Tyr-aT** and **Trp-aT** compared to others.

The histogram of relative ribonucleolytic activities obtained from a precipitation assay at a particular inhibitor concentration (0.5 mM) gave us a clear idea about the comparative inhibitory efficacy of the nucleoside–amino acid conjugates (Fig. 3). It was observed that the compounds with polar amino acid side chains such as **Ser-aT**, **Tyr-aT** and **Trp-aT** (except **His-aT)** were more efficient inhibitors compared to those having hydrophobic side chains (discussed later). Since the active site of RNase A contains ionic residues,[9] **Ser-aT**, **Tyr-aT** and **Trp-aT** with polar side chains are expected to bind more tightly with the active site residues of RNase A compared to others. Further kinetic experiments were conducted with **Ser-aT** and **Tyr-aT**, which showed comparatively good inhibitory activity both in the agarose gel based assay as well

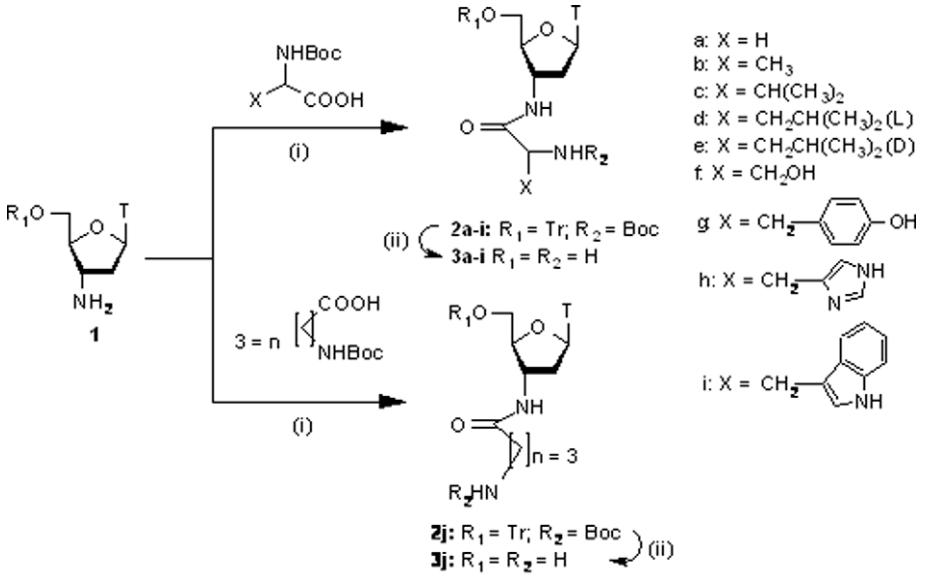

Scheme 1. Synthesis of nucleoside–amino acid conjugates. Reagents and conditions: (i) DCC, DMAP, DMF, 60 h, rt; (ii) TFA in DCM (7:3) 1 h, rt.

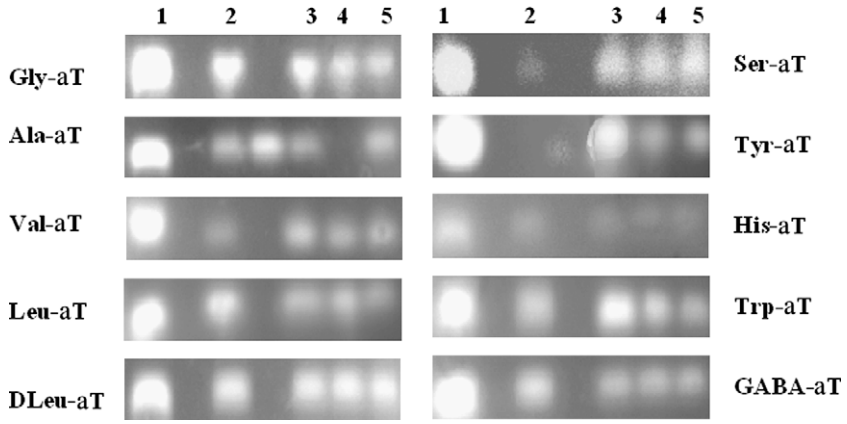

Figure 2. Agarose gel based assay for the inhibition of RNase A. Lane1: tRNA; Lane 2: tRNA and RNase A; Lanes 3, 4 and 5: tRNA and RNase A with decreasing concentration of nucleoside–amino acid conjugates.

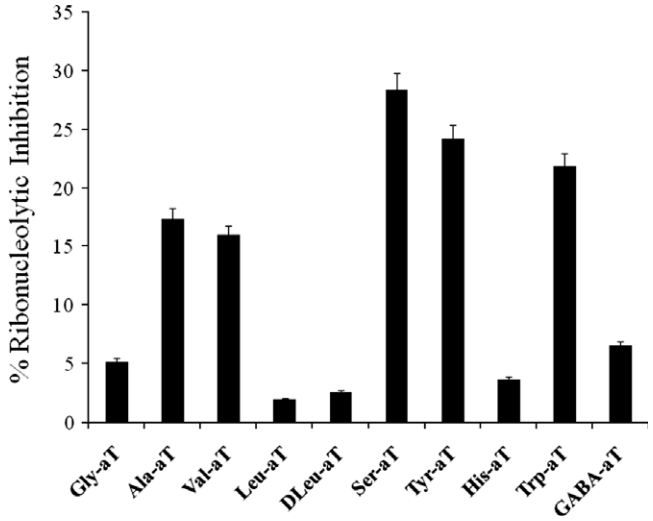

Figure 3. Ribonucleolytic inhibition of RNase A by nucleoside–amino acid conjugates. RNase A and compound concentrations are 0.2 μM and 0.5 mM, respectively.

Table 1
Inhibition constant values of 2′-CMP, 3′-CMP and synthesized compounds

Compounds	Experimental K_i (μM)
3′-CMP	103[11a]
2′-CMP	7[11a]
Ser-aT	80 ± 3
Tyr-aT	451 ± 2

[a] Ref. 11: Review for K_i values of 2′-CMP, 3′-CMP and other nucleotidic inhibitors.

as in the precipitation assay. The inhibition constant values obtained for **Ser-aT** and **Tyr-aT** and those of 2′-CMP and 3′-CMP are presented in Table 1. The nature of the Dixon plots for **Ser-aT** and **Tyr-aT** (Fig. 4A and B, respectively) are indicative of a competitive mode of inhibition. The order of values obtained for the inhibition constants correlate well with those obtained from the precipitation assay.

In order to shed light on the possible orientation of the amino acid counterpart of the nucleoside–amino acid conjugates, a fluorescence experiment was performed in which the fluorophoric property of the **Trp-aT** conjugate was exploited. Since RNase A lacks Trp, excitation at 295 nm would result in excitation and emission from **Trp-aT** alone thus providing important information about the role of the amino acid side chain in binding interaction with RNase A. **Trp-aT** was therefore selected as a compound for monitoring the microenvironment of the fluorophoric indole moiety of tryptophan. Gradual addition of excess RNase A (of same concentration) to **Trp-aT** did not shift the λ_{max} at 363 nm corresponding to the emission band. Negligible quenching was observed even after the addition of excess RNase A in which the final molar ratio of RNase A to **Trp-aT** was over 3:1 (Fig. 5). This experiment clearly indicated that the indole moiety of **Trp-aT** was not in close proximity to the P_1 site of RNase A, which would have led to a shift in λ_{max} of the fluorophore. However, the observed inhibition of the enzymatic activity of RNase A by **Trp-aT** led us to conclude that the amino group rather than the amino acid side chain played a crucial role in ligand–protein complex. Docking studies further substantiated these observations (discussed later).

Keeping these results in mind, we further proceeded to visualize the protein–ligand complexes as obtained from docking studies. Protein ligand docking studies provide an insight into the interaction and mode of binding of the inhibitors with the proteins. Possible hydrogen bonding distances of the ligands with the interacting residues of the RNase A are given in Tables S1–S10 in Supplementary data along with the docking poses (Figs. S1–S10). For the nucleoside–amino acid conjugates having hydrophobic side chains, we have proceeded from **Gly-aT** to **Ala-aT, Val-aT, Leu-aT, DLeu-aT** and **GABA-aT** by concomitant increase in hydrophobicity. In this series the 'free amino group' of **Ala-aT** and **Val-aT** was found to be in the proximity of His-119. However, for the other compounds in this series it was found that the 'free amino group' was not close to the active site histidine residues. The presence of the long hydrophobic side chain of **Leu-aT** and **DLeu-aT** (irrespective of the chirality) results in an unfavorable hydrophobic-ionic interaction. For the series of compounds with polar side chains **Ser-aT**, **Tyr-aT** and **Trp-aT** showed inhibition, **His-aT** being an exception. The reason for this may be as follows. For the purine base to be involved in a favorable stacking interaction with the imidazole moiety of His-119, it is required that Gln-69 forms a hydrogen bond with the nucleobase to position it properly. However, the imidazole moiety of **His-aT** was found to be within hydrogen bonding distance of Gln-69 of RNase A thus likely preventing its free $-NH_2$ group to interact with the active site His residues. The docking poses indicate that the 'free amino groups' of **Ser-aT**, **Tyr-aT** and **Trp-aT** are suitably positioned to interact with His-119. This substantiates the experimental observation of a competitive mode of inhibition from kinetic experiments. In comparison to A**la-aT, Ser-aT** showed an additional interaction involving the side chain hydroxyl group of (O^{γ^1}) with the backbone of Val-118

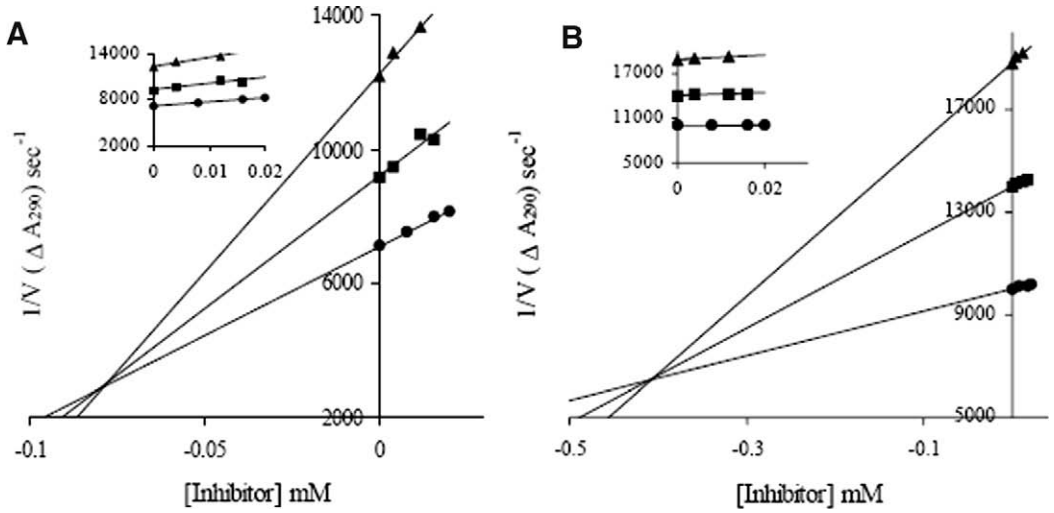

Figure 4. Dixon plot for inhibition of RNase A by (A) **Ser-aT**: substrate concentrations: 0.80 mM (●), 0.64 mM (■) and 0.48 mM (▲); (B) **Tyr-aT**: substrate concentrations: 0.20 mM (●), 0.14 mM (■) and 0.09 mM (▲).

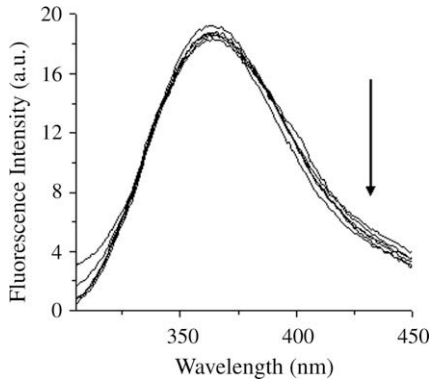

Figure 5. Change of fluorescence intensity of **Trp-aT** (5 μM) with addition of RNase A (17.5 μM). The arrow indicates the progress of titration.

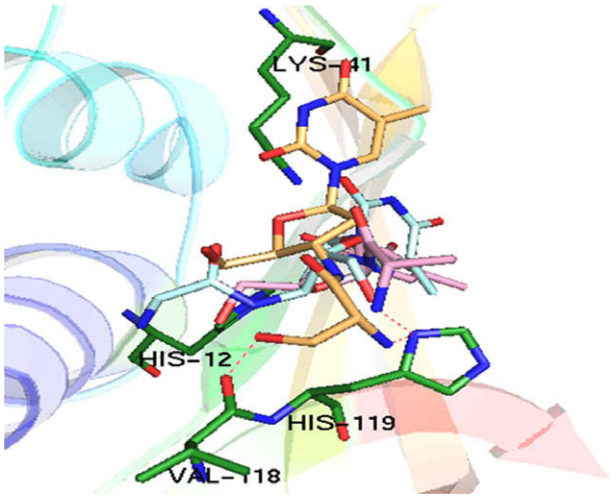

Figure 6. Docking poses of **Gly-aT** (cyan), **Ala-aT** (pink) and **Ser-aT** (orange) with RNase A (1FS3).

(Fig. 6). This interaction with Val-118 brings the 'free amino group' closer to His-119. As a consequence, **Ser-aT** behaves as better inhibitor than A**la-aT** (found in agarose gel and precipitation assay) because of the favorable interaction in the active site cleft. In case of **Trp-aT**, it appears from the docking studies that the indole moiety is not in close proximity to the P1 subsite. This supports the fluorescence studies wherein we observed that the fluorescence emission from the indole moiety of **Trp-aT** is not affected.

To get some insight into the binding pattern of the substrate with the protein, we have compared the interaction of 2′-CMP-RNase A and 3′-CMP-RNase A with the docking conformations of the synthesized compounds. 2′-CMP and 3′-CMP are well known inhibitors of RNase A. The crystal structures of 2′-CMP (1JVU)[16] and 3′-CMP (1RPF)[17] with RNase A show that the phosphate group (for both complexes) makes two hydrogen bonds simultaneously with His-12 and His-119. The corresponding distances from the nearest oxygen atom of the phosphate moiety to the N^{2} of His-12 is 2.56 Å for 2′-CMP and 2.68 Å for 3′-CMP. The distances to the $N^{\delta 1}$ of His-119 are 2.59 Å for 2′-CMP and 3.06 Å for 3′-CMP. It is also observed that the nucleobases are well recognized by the B1 subsite of RNase A indicating a binding pattern similar to the normal substrate of RNase A. However, the binding pattern of our compounds is somewhat different than 2′-CMP and 3′-CMP as observed from docking studies and substantiated by experimental studies (discussed below). Despite their different mode of binding they successfully inhibit the ribonucleolytic activity of RNase A. These observations suggest that slight modifications in the chemical structures of the inhibitors can potentially alter the interaction pattern with the target protein.

To visualize the effect of the inhibitors on the local environment of active site histidines, changes in pK_a of His-12 and His-119 were monitored on complexation of **Ser-aT** and **Leu-aT** with RNase A by ^{1}H NMR experiment. The pK_a values for His-12, His-105 and His-119 were found to be 5.88 ± 0.08, 6.59 ± 0.06 and 6.22 ± 0.03, respectively for free RNase A (red curves in Fig. 7A–C). On addition of **Ser-aT** to RNase A, the pK_a values shifted to 5.91 ± 0.02, 6.58 ± 0.04 and 5.72 ± 0.05, respectively (green curves in Fig. 7A–C). This implies that **Ser-aT** interacted with the active site residues of RNase A, preferentially near His-119 resulting in a distinct shift of its pK_a value. The pK_a values of His-12 and His-105, on the other hand remained essentially unaltered. From this observation, we conclude that the normal protonation/deprotonation equilibrium of the active site residues by the 'free amino group' was disrupted on binding. The decrease in pK_a of His-119 suggests that it was surrounded by positively charged species. From the docking study it was also found that the 'free amino group' of **Ser-aT** formed a

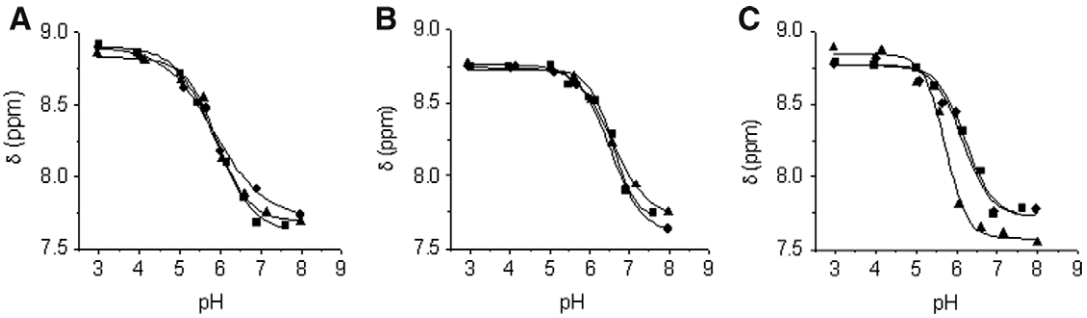

Figure 7. pH dependence of C-2 proton signals. (A) His-12, (B) His-105, (C) His-119. Chemical shifts for RNase A (■), for compound **Leu-aT** (●) and for compound **Ser-aT** (▲).

hydrogen bond with His-119. Since the pK_a value of His-119 is lower than the pK_a of the 'free amino group' (~9 to 10), so it influenced His-119 (behaves as acidic entity in catalysis mechanism) to dissociated. Thereafter, the amino group got ionized to $-NH_3^+$ ion and formed a hydrogen bond with His-119. This observation is in contrast to that found in case of phosphate functionalized nucleotides (e.g., increase of pK_a value for 2′-CMP and 3′-CMP) as reported earlier.[18,19]

Phosphate esters resulted in a greater increase in the pK_a of active site histidine residues because of the better alignment of two anionic oxygen atoms of the phosphate moiety. Their perfect alignment helps them to form strong hydrogen bond with active site residues than the molecules reported here. To support our speculation regarding the pK_a perturbation, we chose **Leu-aT,** which did not show any inhibition of RNase A. From the ^{1}H NMR titration of RNase A-**Leu-aT** complex we found that the pK_a values of His-12, His-105 and His-119 changed from 5.88 ± 0.08, 6.59 ± 0.06 and 6.22 ± 0.03 (of RNase A) to 5.88 ± 0.02 6.54 ± 0.05 and 6.18 ± 0.03, respectively (blue curve in Fig. 7A–C). Almost unchanged pK_a values implied that **Leu-aT** was not able to perturb the pK_a of the active site histidine residues in ligand–protein complex. This may be due to the presence of the large hydrophobic moiety of **Leu-aT** that prevented the entry into the polar active site cleft, which is essentially hydrophilic in nature.

Nucleoside–amino acid conjugates are shown to inhibit the ribonucleolytic activity of RNase A for the first time. Although these compounds contain a 'free amino group' the inhibition properties were found to depend also on the side chain counterpart of the amino acid moiety. Since the active site of the enzyme is ionic in nature, polar conjugates such as **Ser-aT** and **Tyr-aT** were found to be more effective inhibitors. Kinetic experiments indicate competitive inhibition by **Ser-aT** which was also found to preferentially perturb the microenvironment of His-119 during binding with RNase A as observed from ^{1}H NMR studies. The decrease in pK_a values for His-119 is indicative of its interaction with the 'free amino group' of the inhibitors. Docking studies further substantiated these experimental observations.

3. Materials and methods

3.1. Materials

Bovine pancreatic RNase A, yeast tRNA, 2′,3′-cCMP, 3′-CMP, human serum albumin (HSA), 3-trimethylsilylpropane sulfonic acid (DSS) and D_2O were from Sigma–Aldrich. All other reagents were from SRL India. Column chromatographic separations were performed using silica gel (60–120 and 230–400 mesh). Solvents were dried and distilled following standard procedures. TLC was carried out on precoated plates (Merck Silica Gel 60, f_{254}), and the spots visualized with UV light or by charring the plates dipped in 5% H_2SO_4–MeOH solution or 5% H_2SO_4/vanillin/EtOH or 5% ninhydrin in MeOH solution. ^{1}H NMR (400 MHz) and ^{13}C NMR (100 MHz) spectra were recorded on a Bruker NMR spectrometer δ scale). UV–Vis measurements were made using a Perkin Elmer UV–Vis spectrophotometer (Model Lambda 25). Fluorescence measurements were recorded on a Spex Fluorolog-3 machine. Concentrations of the solutions were determined spectrophotometrically using the following data: $\varepsilon_{278.5}$ (RNase A),[20] ε_{268} (2′,3′-cCMP)[21] are 9800 and 8500 $M^{-1}\,cm^{-1}$, respectively.

3.2. Synthesis of nucleoside–amino acid conjugates

3.2.1. General procedure for the synthesis of compounds 2a–j

Compound **1**[22,23] (1 mmol) and the *N*-BOC-protected amino acids (1 mmol) were suspended in dry DMF (15 ml) and cooled to −15 °C. Thereafter, DMAP (1 mmol) and DCC (1 mmol) were added consecutively and the mixture was stirred for 48 h at room temperature. After completion of the reaction, the mixture was filtered and washed with ethyl acetate. The filtrate was stirred with saturated $NaHCO_3$ solution and extracted with ethyl acetate. Combined organic layers were evaporated under reduced pressure. Crude residues thus obtained were purified over silica gel to afford compounds **2a**–**j**. Synthesis of compounds **2a**, **2b** and **2g** were reported earlier.[24]

3.2.2. General procedure for the synthesis of compounds 3a–j

Compounds **2a**–**j** were stirred with 70% trifluoroacetic acid in DCM for 1 h at room temperature. All volatile matters were removed under reduced pressure. Crude residues thus obtained were purified over silica gel to afford the required nucleoside–amino acid conjugates, **3a**–**j**.

3.2.2.1. 2′,3′-Dideoxy-3′-glycylamino thymidine 3a (Gly-aT). Compound **2a** (0.1 g, 0.16 mmol) was converted to **3a** (0.03 g, 64%) following the general procedure. ^{1}H NMR: (D_2O): δ 1.9 (s, 3H), 2.41–2.49 (m, 2H), 3.44 (bs, 2H), 3.74 (dd, J = 3.2, 12.4 Hz, 1H), 3.87 (m, 1H), 3.99 (bs, 1H), 4.53 (m, 1H), 6.25 (t, J = 5.2 Hz, 1H), 7.7 (s, 1H). ^{13}C NMR (D_2O + DMSO-d_6): δ 13.2, 38.0 (CH_2), 44.5 (CH_2), 50.1, 62.3 (CH_2), 85.6, 86.2, 112.8, 139.1, 153.2, 168.1, 174.9. HRMS (ESI^+): m/z calcd for $C_{12}H_{19}N_4O_5$ $[M+H]^+$: 299.1355; found: 299.1351.

3.2.2.2. 2′,3′-Dideoxy-3′-L-alanylamino thymidine 3b (Ala-aT). Compound **2b** (0.32 g, 0.49 mmol) was converted to **3b** (0.09 g, 59%) following the general procedure. ^{1}H NMR: (DMSO-d_6): δ 1.12 (d, J = 6.4 Hz, 3H), 1.78 (s, 3H), 2.12–2.24 (m, 2H), 3.27 (m, 1H), 3.53 (m, 1H), 3.62 (m, 1H), 3.77 (bs, 1H), 4.32 (bs, 1H), 6.19 (t, J = 6.4 Hz, 1H), 7.77 (s, 1H). ^{13}C NMR (DMSO-d_6): δ 12.6, 21.6, 37.4 (CH_2), 49.1, 50.4, 61.6 (CH_2), 83.9, 85.3, 109.8, 136.6, 150.8, 164.1, 176.0. HRMS (ESI^+): m/z calcd for $C_{13}H_{21}N_4O_5$ $[M+H]^+$: 313.1512; found: 313.1502.

3.2.2.3. 2′,3′-Dideoxy-3′-L-valinylamino thymidine 3c (Val-aT). Compound **2c** (0.52 g, 0.49 mmol) was converted to **3c** (0.10 g, 52%) following the general procedure. ^{1}H NMR: (DMSO-d_6): δ 0.81 (dd, J = 6.8, 23.2 Hz, 6H), 1.77–1.86 (m, 4H), 2.09–2.23 (m, 2H), 2.89 (d, J = 5.2 Hz, 1H), 3.51–3.63 (m, 2H), 3.76 (bs, 1H), 4.34 (bs, 1H), 6.17 (t, J = 6.4 Hz, 1H), 7.76 (s, 1H). ^{13}C NMR (DMSO-d_6): δ 12.6, 17.8, 19.9, 32.2, 37.4 (CH_2), 49.1, 60.3, 61.6 (CH_2), 83.9, 85.4, 109.8, 136.6, 150.8, 164.1, 175.0. HRMS (ESI$^+$): m/z calcd for $C_{15}H_{25}N_4O_5$ [M+H]$^+$: 341.1825; found: 341.1808.

3.2.2.4. 2′,3′-Dideoxy-3′-L-leucylamino thymidine 3d (Leu-aT). Compound **2d** (0.50 g, 0.72 mmol) was converted to **3d** (0.20 g, 78%) following the general procedure. ^{1}H NMR: (D_2O): δ 0.95 (m, 6H), 1.62–1.76 (m, 3H), 1.90 (s, 3H), 2.41–2.54 (m, 2H), 3.73 (dd, J = 4.4, 12.8 Hz, 1H), 3.86 (dd, J = 2.8, 12.8 Hz, 1H), 3.96–4.02 (m, 2H), 4.56 (q, J = 7.6 Hz, 1H), 6.25 (q, J = 5.2 Hz, 1H), 7.70 (s, 1H). ^{13}C NMR (D_2O + DMSO-d_6): δ 13.2, 22.8, 23.3, 25.5, 37.8 (CH_2), 41.5 (CH_2), 50.5, 53.5, 62.3 (CH_2), 85.4, 86.3, 112.9, 139.1, 153.1, 167.9, 172.0. HRMS (ESI$^+$): m/z calcd for $C_{16}H_{27}N_4O_5$ [M+H]$^+$: 355.1981; found: 355.1950.

3.2.2.5. 2′,3′-Dideoxy-3′-D-leucylamino thymidine 3e (DLeu-aT). Compound **2e** (0.25 g, 0.36 mmol) was converted to **3e** (0.11 g, 86%) following the general procedure. ^{1}H NMR: (D_2O): δ 0.94 (m, 6H), 1.64–1.76 (m, 3H), 1.91 (s, 3H), 2.41–2.51 (m, 2H), 3.76 (dd, J = 4.4, 12.8 Hz, 1H), 3.85–3.9 (m, 1H), 3.96 (t, J = 7.2 Hz, 1H), 4.04–4.12 (m, 1H), 4.55 (q, J = 7.2 Hz, 1H), 6.25 (t, J = 6 Hz, 1H), 7.70 (s, 1H). ^{13}C NMR (D_2O + DMSO-d_6): δ 13.2, 22.8, 23.4, 25.5, 37.8 (CH_2), 41.5 (CH_2), 50.5, 53.5, 62.3 (CH_2), 85.4, 89.3, 112.9, 139.1, 153.1, 167.9, 172.1. HRMS (ESI$^+$): m/z calcd for $C_{16}H_{27}N_4O_5$ [M+H]$^+$: 355.1981; found: 355.1980.

3.2.2.6. 2′,3′-Dideoxy-3′-L-serinylamino thymidine 3f (Ser-aT). Compound **2f** (0.09 g, 0.13 mmol) was converted to **3f** (0.02 g, 45%) following the general procedure. ^{1}H NMR: (D_2O): δ 1.79 (s, 3H), 2.32–2.39 (m, 2H), 3.44 (t, J = 5.2 Hz, 1H), 3.61–3.65 (m, 3H), 3.75 (dd, J = 2.8, 12.8 Hz, 1H), 3.90 (m, 1H), 4.42 (q, J = 7.6 Hz, 1H), 6.15 (t, J = 5.2 Hz, 1H), 7.60 (s, 1H). ^{13}C NMR (D_2O + DMSO-d_6): δ 12.2, 36.9 (CH_2), 48.7, 56.6, 61.2 (CH_2), 64.0 (CH_2), 83.4, 84.9, 109.4, 136.2, 150.4, 163.7, 173.1. HRMS (ESI$^+$): m/z calcd for $C_{13}H_{21}N_4O_6$ [M+H]$^+$: 329.1349; found: 329.1353.

3.2.2.7. 2′,3′-Dideoxy-3′-L-tyrosylamino thymidine 3g (Tyr-aT). Compound **2g** (0.18 g, 0.24 mmol) was converted to **3g** (0.05 g, 51%) following the general procedure. ^{1}H NMR: (DMSO-d_6): δ 1.76 (s, 3H), 2.04–2.19 (m, 2H), 2.49–2.75 (m, 2H), 3.28 (t, J = 6.4 Hz, 2H), 3.45–3.62 (m, 2H), 4.30 (bs, 1H), 6.14 (t, J = 6.4 Hz, 1H), 6.63 (m, 2H), 6.95 (m, 2H), 7.74 (s, 1H). ^{13}C NMR (DMSO-d_6): δ 12.7, 37.4 (CH_2), 40.9 (CH_2), 49.0, 56.8, 61.6 (CH_2), 83.8, 85.3, 109.8, 115.3, 128.8, 130.5, 136.6, 150.8, 156.1, 164.1, 174.8. HRMS (ESI$^+$): m/z calcd for $C_{19}H_{25}N_4O_6$ [M+H]$^+$: 405.1742; found: 405.1731.

3.2.2.8. 2′,3′-Dideoxy-3′-L-histidinylamino thymidine 3h (His-aT). Compound **2h** (0.16 g, 0.22 mmol) was converted to **3h** (0.05 g, 57%) following the general procedure. ^{1}H NMR: (D_2O): δ 1.87 (s, 3H), 2.31–2.48 (m, 2H), 3.08–3.21 (m, 2H), 3.56–3.59 (m, 1H), 3.63–3.74 (m, 2H), 4.03–4.20 (m, 1H), 4.36–4.43 (m, 1H), 6.08–6.16 (m, 1H), 7.12 (s, 1H), 7.64 (s, 1H), 7.95 (s, 1H). ^{13}C NMR (D_2O + DMSO-d_6): δ 13.6, 17.4, 42.0 (CH_2), 50.5 (CH_2), 54.4, 57.9, 66.3 (CH_2), 88.7, 89.9, 114.6, 140.3, 141.3, 155.5, 168.9, 173.2, 173.3. HRMS (ESI$^+$): m/z calcd for $C_{16}H_{23}N_6O_5$ [M+H]$^+$: 379.1730; found: 379.1698.

3.2.2.9. 2′,3′-Dideoxy-3′-L-tryptophanylamino thymidine 3i (Trp-aT). Compound **2i** (0.15 g, 0.19 mmol) was converted to **3i** (0.04 g, 47%) following the general procedure. ^{1}H NMR: (DMSO-d_6): δ 1.76 (s, 3H), 2.02–2.16 (m, 2H), 2.81–2.9 (m, 1H), 3.03–3.08 (m, 1H), 3.40–3.44 (m, 1H), 3.52–3.59 (m, 3H), 4.31 (bs, 1H), 6.13 (t, J = 6.8 Hz, 1H), 6.93–7.06 (m, 2H), 7.13 (s, 1H), 7.32 (m, 1H), 7.55 (m, 1H), 7.75 (s, 1H). ^{13}C NMR (DMSO-d_6): δ 12.7, 29.4 (CH_2), 37.4 (CH_2), 49.1, 55.7, 61.6 (CH_2), 83.8, 85.2, 109.8, 111.7, 118.6, 118.9, 121.3, 124.2, 127.8, 136.6, 136.6, 136.7, 150.8, 164.1, 175.0. HRMS (ESI$^+$): m/z calcd for $C_{21}H_{26}N_5O_5$ [M+H]$^+$: 428.1934; found: 428.1934.

3.2.2.10. 2′,3′-Dideoxy-3′-(γ-aminobutyric acid)amino thymidine 3j (GABA-aT). Compound **2j** (0.10 g, 0.14 mmol) was converted to **3j** (0.03 g, 58%) following the general procedure. ^{1}H NMR: (D_2O): δ 0.96 (m, 3H), 1.83–1.91 (m, 5H), 2.43–2.52 (m, 2H), 3.72–3.78 (m, 2H), 3.87 (dd, J = 2.8, 12.8 Hz, 1H), 3.99–4.02 (m, 1H), 4.55 (m, 1H), 6.24 (q, J = 5.2 Hz, 1H), 7.70 (s, 1H). ^{13}C NMR (D_2O + DMSO-d_6): δ 10.2, 13.2, 26.7 (CH_2), 37.9 (CH_2), 50.3, 56.2, 62.3 (CH_2), 85.6, 86.3, 112.9, 139.1, 153.1, 167.9, 173.3. HRMS (ESI$^+$): m/z calcd for $C_{14}H_{23}N_4O_5$ [M+H]$^+$: 327.1668; found: 327.1660.

3.3. Agarose gel-based assay

Inhibition of RNase A by all nucleoside–amino acid conjugates was checked qualitatively by the degradation of tRNA in an agarose gel. In this method, 20 μl of RNase A (0.66 μM) was mixed with 10, 15 and 20 μl of the compounds (0.92 mM) to a final volume of 50 μl and the resulting solutions were incubated for 6 h at 37 °C. 20 μl aliquots from incubated mixtures were then mixed with 20 μl of tRNA solution (5.0 mg/ml) and 10 μl of sample buffer (containing 10% glycerol and 0.025% bromophenol blue). The mixture was then incubated for another 30 min. A volume of 15 μl from each solution were extracted and loaded onto a 1.1% agarose gel. The gel was run in 0.04 M Tris-acetic acid-EDTA (TAE) buffer (pH 8.0). The undegraded tRNA was visualized by ethidium bromide staining under UV light.

3.4. Precipitation assay

Inhibition of the ribonucleolytic activity of RNase A was quantified by the precipitation assay as described by Bond.[25] In this method 10 μl of RNase A (2 μM) was mixed with 50 μl of each nucleoside–amino acid conjugate (1 mM) to a final volume of 100 μl and incubated for 2 h at 37 °C. A 20 μl aliquot of the resulting solutions from the incubated mixtures were then mixed with 40 μl of tRNA (5 mg/ml), 40 μl of Tris–HCl buffer of pH 7.5 containing 5 mM EDTA and 0.5 mg/ml HSA. After incubation of the reaction mixture at 25 °C for 30 min, 200 μl of ice-cold 1.14 (N) perchloric acid containing 6 mM uranyl acetate was added to quench the reaction. The solution was then kept in ice for another 30 min and centrifuged at 4 °C at 12000 rpm for 5 min. A 100 μl aliquot of the supernatant was taken and diluted to 1 ml. The change in absorbance at 260 nm was measured and compared to a control set. Based on the results obtained, further experiments were carried out with the compounds showing substantial inhibition potency.

3.5. Inhibition kinetics

The inhibition of RNase A by Ser-aT and Tyr-aT was assessed individually by a spectrophotometric method as described by Anderson and co-workers.[21] The assay was performed in oligovinylsulfonic acid free[26] 0.1 M Mes-NaOH buffer, pH 6.0 containing 0.1 M NaCl using 2′,3′-cCMP as the substrate. For Ser-aT, the inhibitor concentration was ranged from 0 to 20 μM and the substrate concentration was used from 0.48 to 0.80 mM. For Tyr-aT, the inhibitor

concentration was ranged from 0 to 100 μM with substrate concentrations from 0.09 to 0.20 mM. The RNase A concentration was 12 μM. The inhibition constants (K_i) were determined from initial velocity data. The reciprocal of initial velocity was plotted against the inhibitor concentration (Dixon Plot) according to the equation:

$$\frac{1}{v} = \frac{K_m}{V_{max}[S]K_i}[I] + \frac{1}{V_{max}}\left[1 + \frac{K_m}{[S]}\right]$$

where, v is the initial velocity, [S] the substrate concentration, [I] the inhibitor concentration, K_m the Michaelis constant, K_i the inhibition constant and V_{max} the maximum velocity.

3.6. Fluorescence study

Fluorimetric titrations were performed in a 1 cm quartz cuvette using an excitation wavelength of 295 nm. 2.5 ml of 5 μM Trp-aT in 20 mM phosphate buffer pH 7.0 containing 50 mM NaCl was titrated by successive addition of RNase A to reach a final protein concentration of 17.5 μM. The emission spectra were recorded from 305 to 450 nm with a slit width of 5 nm for both the excitation and emission beams.

3.7. Docking studies of the nucleoside–amino acid conjugates

The crystal structure of RNase A (PDB entry 1FS3) was downloaded from the Protein Data Bank.[27] The 3D structures of the nucleoside–amino acid conjugates were generated by SYBYL6.92 (Tripos Inc., St. Louis, USA) and their energy-minimized conformations were obtained with the help of the TRIPOS force field using Gasteiger-Hückel charges with a gradient of 0.005 kcal/mol. The FlexX software as part of the SYBYL suite was used for docking of the nucleoside–amino acid conjugates with RNase A. PyMol[28] was used for visualization of the docked conformations.

3.8. ^{1}H NMR Study for proton association–dissociation equilibrium

Exchangeable hydrogen atoms of RNase A were replaced by deuterium to ease the pH titration for the ^{1}H NMR study. To exchange hydrogen by deuterium the protein was dissolved in D_2O and incubated at 50 °C for 20 min and then lyophilized following the method of Quirk and Raines.[29] This was repeated three times. The lyophilized protein was dissolved in D_2O containing 0.17 M NaCl and 0.5 mM DSS. DCl and NaOD solutions were used to adjust the pH* for the range of 3–8, where pH* is the direct measure of the pH which was not corrected for a deuterium isotope effect. The ligand to enzyme molar ratio was 5:1, which was maintained for both compounds Leu-aT and Ser-aT. ^{1}H NMR data were recorded on a Bruker 400 MHz spectrometer at 22.5 °C. The acquisition time was 2 s with 100 scans. The observed δ value was recorded with respect to DSS. The values of δ_{obs} for histidine C-2 protons at different pH were fitted in the following equations:

(a)

$$\delta_{obs} = \delta_0 + \frac{\Delta \times 10^{(pK-pH)}}{1 + 10^{(pK-pH)}} \quad (1)$$

where, δ_{obs} is the observed chemical shift, δ_0 is the chemical shift of the unprotonated form and Δ is the chemical shift change upon protonation.

(b) In the cases where an acid inflection was present the equation:

$$\delta_{obs} = \delta_0 + \frac{\Delta_1 \times 10^{(pK_1-pH)}}{1 + 10^{(pK_1-pH)}} + \frac{\Delta_2 \times 10^{(pK_2-pH)}}{1 + 10^{(pK_2-pH)}} \quad (2)$$

where, Δ_1 and Δ_2 are the chemical shift changes for the acid pH inflection (pK_1) and the basic pH inflection (pK_2), respectively.

Eq. 1 was used for the calculation of pK_a for His-105 and Eq. 2 was used for better fit of the calculated curve of the experimental points obtained for His-12 and His-119, if the existence of an acid inflection is accepted. The titration curve His-48 which is inaccessible to solvent shows anomalous behavior with pH, preventing determination of its pK_a value as was reported earlier.[30] Using Eq. 2 pK_1 and pK_2 are obtained. The large error in the estimated pK_1 values is generally encountered in all cases due to the uncertainty in the experimental points which is close to the width of the acid inflection as reported earlier.[31] Hence for our discussion of pK_a only pK_2 was considered.

Acknowledgments

J.D. thanks CSIR, India for a fellowship. S.D. and T.P. are grateful to the Department of Science and Technology (DST), New Delhi, India, for financial support. J.D. thanks Dr. Kalyan S. Ghosh for his help in some of the experiments.

Supplementary data

Supplementary data associated with this article can be found, in the online version, at doi:10.1016/j.bmc.2009.06.002.

References and notes

1. Fett, J. W.; Strydom, D. J.; Lobb, R. R.; Alderman, E. M.; Bethune, J. L.; Riordan, J. F.; Vallee, B. L. *Biochemistry* **1985**, *24*, 5480.
2. Sorrentino, S.; Glitz, D. G.; Hamann, K. J.; Loegering, D. A.; Checkel, J. L.; Gleich, G. J. *J. Biol. Chem.* **1992**, *267*, 14859.
3. D'Alessio, G.; Di Donato, A.; Piccoli, A. *Trends Biochem. Sci.* **1991**, *16*, 104.
4. Shapiro, R.; Weremowicz, S.; Riordan, J. F.; Vallee, B. L. *Proc. Natl. Acad. Sci. U.S.A.* **1987**, *84*, 8783.
5. Hamann, K. J.; Barker, R. L.; Loegering, D. A.; Pease, L. R.; Gleich, G. J. *Gene* **1989**, *83*, 161.
6. D'Alessio, G.; Di Donato, A.; Mazzarella, L.; Piccoli, R. In *Ribonucleases Structures and Functions*; D'Alessio, G., Riordan, J. F., Eds.; Academic Press: New York, 1997; pp 383–423.
7. Shapiro, R.; Riordan, J. F.; Vallee, B. L. *Biochemistry* **1986**, *25*, 3527.
8. Nogués, M. V.; Vilanova, M.; Cuchillo, C. M. *Biochim. Biophys. Acta* **1995**, *1253*, 16.
9. Raines, R. T. *Chem. Rev.* **1998**, *98*, 1045.
10. Witzel, H.; Barnard, E. A. *Biochem. Biophys. Res. Commun.* **1962**, *7*, 295.
11. Russo, N.; Acharya, K. R.; Shapiro, R. *Methods Enzymol.* **2001**, *341*, 629.
12. Yakovlev, G. I.; Mitkevich, V. A.; Makarov, A. A. *Mol. Biol.* **2006**, *40*, 867.
13. Maiti, T. K.; De, S.; Dasgupta, S.; Pathak, T. *Bioorg. Med. Chem.* **2006**, *14*, 1221.
14. Leonidas, D. D.; Maiti, T. K.; Samanta, A.; Dasgupta, S.; Pathak, T.; Zographos, S. E.; Oikonomakos, N. G. *Bioorg. Med. Chem.* **2006**, *14*, 6055.
15. Ghosh, K. S.; Debnath, J.; Pathak, T.; Dasgupta, S. *Bioorg. Med. Chem. Lett.* **2008**, *18*, 5503.
16. Vitagliano, L.; Merlino, A.; Zagari, A.; Mazzarella, L. *Proteins* **2002**, *46*, 97.
17. Zegers, I.; Maes, D.; Dao-Thi, M. H.; Poortmans, F.; Palmer, R.; Wyns, L. *Protein Sci.* **1994**, *3*, 2322.
18. Meadows, D. H.; Roberts, G. C. K.; Jardetzky, O. *J. Mol. Biol.* **1969**, *45*, 491.
19. Meadows, D. H.; Jardetzky, O. *Proc. Natl. Acad. Sci. U.S.A.* **1968**, *61*, 406.
20. Sela, M.; Anfinsen, C. B. *Biochim. Biophys. Acta* **1957**, *24*, 229.
21. Anderson, D. G.; Hammes, G. G.; Walz, F. G. *Biochemistry* **1968**, *7*, 1637.
22. Batra, M.; Romea, P.; Urpí, F.; Vilarrrasa, J. *Tetrahedron* **1990**, *46*, 587.
23. Herdewijin, P.; Balzarini, J.; Baba, M.; Pauwels, R.; Van Aerschot, A.; Janssen, G.; De Clercq, E. *J. Med. Chem.* **1988**, *31*, 2040.
24. Wengel, J.; Motawia, M. S.; Pedersen, E. B.; Nielsen, C. M. *J. Heterocycl. Chem.* **1992**, *29*, 5.
25. Bond, M. D. *Anal. Biochem.* **1988**, *173*, 166.
26. Smith, B. D.; Soellner, M. B.; Raines, R. T. *J. Biol. Chem.* **2003**, *278*, 20934.
27. Berman, H. M.; Westbrook, J.; Feng, Z.; Gilliland, G.; Bhat, T. N.; Weissig, H.; Shindyalov, I. N.; Bourne, P. E. *Nucleic Acids Res.* **2000**, *28*, 235.
28. DeLano, W. L. The PyMOL Molecular Graphics System, DeLano Scientific, San Carlos, CA, 2004. USA. http://pymol.sourceforge.net/.
29. Quirk, D. J.; Raines, R. T. *Biophys. J.* **1999**, *76*, 1571.
30. Markley, J. L. *Biochemistry* **1975**, *14*, 3554.
31. Arús, C.; Paolillo, L.; Llorens, R.; Napolitano, R.; Parés, X.; Cuchillo, C. M. *Biochim. Biophys. Acta* **1981**, *660*, 117.